Results in Engineering 17 (2023) 100844

Contents lists available at ScienceDirect

Results in Engineering

journal homepage: www.sciencedirect.com/journal/results-in-engineering

Analysis of the effect of ventilation hole angle and material variation on thermal behavior for car disc brakes using the finite element method

Mohammad Tauviqirrahman [a,*], M. Muchammad [a], Tian Setiazi [a], Budi Setiyana [a,b], J. Jamari [a]

[a] Laboratory for Engineering Design and Tribology, Department of Mechanical Engineering, Diponegoro University, Jl. Soedharto SH, Tembalang, Semarang 50275, Indonesia

[b] Laboratory for Surface Technology and Tribology, Faculty of Engineering Technology, University of Twente, Drienerlolaan 5, Postbus 217, 7500 AE Enschede, the Netherlands

ARTICLE INFO

Keywords:
Disc brake
Finite element analysis
Heat dissipation
Ventilation angle

ABSTRACT

Brakes are used to slow down or stop a moving object. The temperature of the disc brake will rise as a result of the conversion of kinetic energy from vehicle speed into thermal energy during the braking operation. To prevent harm to the disc brake or other components, the heat generated by this disc brake must then be released into the environment. Therefore, it is crucial to provide effective heat dissipation to the environment. Increasing the surface area where heat is dissipated into the environment is one potential solution. In this study, the variation of the drill hole angles and groove hole angles is proposed as a geometry modification to encourage greater heat dissipation in disc brakes. In addition, the thermal performance of disc brakes made from various types of materials is assessed using finite element analysis. The materials employed are carbon ceramic, stainless steel, and gray cast iron. The numerical findings show that the groove-type disc brake with a ventilation hole angle of 0° angle has the lowest maximum temperature. In addition, it is revealed that the disc brake made of gray cast iron material results in the lowest peak temperature. The numerical results also indicate that due to the thinning of the geometry, the addition of the ventilation hole angle contributes to the phenomena of temperature concentration in specific areas of the disc brake. This study demonstrates that disc brake material and ventilation hole play a significant effect in altering the thermal characteristics.

1. Introduction

Brakes are necessary and critical mechanical parts that help a car stop in any circumstance [1]. The brake's function is to absorb the kinetic energy of the moving element. Due to the friction between the disc and pad, the kinetic energy (accumulated in the vehicle as a result of its speed) is converted into thermal energy, which is then gradually dissipated to the environment by natural convection [2]. The four essential parts of a disc brake are the housing for the pistons, calipers, the brake disc, and the brake pads [3–8]. Because temperature affects the thermo-mechanical behavior of the structure, thermal analysis is a fundamental step in the study of brake systems [9].

The ability to ensure quick heat dissipation into the atmosphere is the primary feature of brake discs. The brake system becomes overheated, which reduces braking effectiveness [10]. The uneven distribution of heat to the disc brake material might result in cracks. The disc brake will uniformly expand in response to a non-uniform temperature distribution, leading to a concentration of thermal stress and crack propagation that harms the disc. Numerous experts have spent years studying the complicated phenomena of heat dissipation on the disc brake, which has a direct impact on braking performance [11–15]. Belhocine and Bouchetara [16] examined both a full and a ventilated disc when analyzing the thermal behavior of a disc in a transient state. Based on numerical simulation, it was shown that radial ventilation is essential in keeping the disc cool during braking operations. Sarkar and Rathod [17] presented an interesting review of the thermal analysis of ventilated disc brakes by varying design parameters. They highlighted that angled vanes and vanes of varying lengths appear to have better heat dissipation in car brakes. Dhir et al. [18] performed a steady-state thermal study and a structural analysis on three disc brakes with varying weights and geometric designs. Through this investigation, it has been determined that the ventilation provided by the airfoils and the perforations play a crucial part in the cooling of the disc. Studying the aerodynamic losses of several disc brake designs, Gerlici et al. [19] found that solid rotors had the lowest aerodynamic losses while disc

* Corresponding author.
E-mail address: mohammad.tauviqirrahman@ft.undip.ac.id (M. Tauviqirrahman).

https://doi.org/10.1016/j.rineng.2022.100844
Received 3 October 2022; Received in revised form 5 December 2022; Accepted 13 December 2022
Available online 20 December 2022

Nomenclature

A	Area, m^2
C_p	Specific heat, J/kg.°C
d_0	Shaft diameter of disc brake, mm
d_1	Wheel nut diameter, mm
d_2	Drill hole diameter, mm
E	Elastic modulus, GPa
$\dot{E}$	Heat rate due to friction, W
$\dot{E}_d$	Heat rate due to friction on disc, W
$\dot{E}_p$	Heat rate due to friction on pad, W
F_f	Friction force, N
g_1	Diameter of groove hole, deg
g_2	Arc length of groove hole, mm
h	Convection heat transfer coefficient, $W/m^2.°C$
k	Thermal conductivity, W/m.°C
L_1	Distance of drill hole 1 from shaft, mm
L_2	Distance of drill hole 2 from shaft, mm
L_3	Distance of drill hole 3 from shaft, mm
L_4	Distance of drill hole 4 from shaft, mm
L_5	Initial distance of groove hole to shaft, mm
L_6	Final distance of groove hole to shaft, mm
p	Pressure, N/m^2
$Pmax$	Maximum pressure, N/m^2
Q	Heat transfer rate, W
q_{01}	Initial heat flux on pad, W/m^2
q_{02}	Initial heat flux on disc, W/m^2
q_1	Heat flux on pad, W/m^2
q_2	Heat flux on disc, W/m^2
$q_{2,CC}$	Heat flux on carbon ceramic disc, W/m^2
$q_{2,GCI}$	Heat flux on gray cast iron discs, W/m^2
$q_{2,ss420}$	Heat flux on stainless steel disc, W/m^2
r_1	Inner radius in disc, mm
r_2	Outer radius in disc, mm
r_3	Inner radius in pad, mm
r_4	Outer radius in pad, mm
S_d	Disc friction contact surface, m^2
S_p	Pad friction contact surface, m^2
T	Disc brake thickness, mm
t	Time, s
T_∞	Environmental temperature, °C
t_b	Braking time, s
T_w	Surface temperature, °C
V	Relative shear speed, m/s

Greek Symbol

α_1	Drill hole distance 2 to 1, mm
α_2	Drill hole distance 3 to 1, mm
α_3	Drill hole distance 4 to 1, mm
θ	Drill hole and groove hole tilt angle, deg
μ	Friction coefficient
ν	Poisson ratio
ν_d	Poisson ratio of disc
ν_p	Poisson ratio of pad
ξ	Thermal effusivity, $J/m^2.°C.s^{0.5}$
ξ_d	Thermal effusivity of disc, $J/m^2.°C.s^{0.5}$
ξ_p	Thermal effusivity of pad, $J/m^2.°C.s^{0.5}$
$\xi_{d,GCI}$	Thermal effusivity of gray cast iron disc $J/m^2.°C.s^{0.5}$
$\xi_{d,ss420}$	Thermal effusivity of stainless steel disc, $J/m^2.°C.s^{0.5}$
$\xi_{d,cc}$	Thermal effusivity of carbon ceramic disc, $J/m^2.°C.s^{0.5}$
ρ	Density, kg/m^3
ρ_d	Density of disc, kg/m^3
ρ_p	Density of pad, kg/m^3
σ_y	Tensile strength, MPa
φ_0	Arc angle pad, deg
ω	Wheel speed, rad/s
ω_0	Wheel initial speed, rad/s
ϖ	Heat partition coefficient
ϖ_{GCI}	Heat partition coefficient of gray cast iron
ϖ_{ss420}	Heat partition coefficient of stainless steel
ϖ_{cc}	Heat partition coefficient of carbon ceramic

Abbreviations

ASTM	American Standard Testing and Material
GCI	Gray Cast Iron
CC	Carbon Ceramic
SS	Stainless Steel

Fig. 1. Three-dimensional solid-type disc brake.

brakes with vents and vanes have the largest losses. Radial vane designs have the highest losses. Similarly, Choudhary et al. [20] performed a study by varying the ventilation hole angle on the disc brake of a motorbike. They concluded that as the ventilation hole angle on the disc brake increases, the maximum temperature and deformation linearly reduce. When compared to conventional disc brake rotors, discs with a 7° angle variation offer approximately 30% reductions in maximum temperature, approximately 47% reductions in maximum deformation, and approximately 13% reductions in maximum stress. All of these researches have made significant contributions to the state of disc brake performance. However, research on car disc brakes with drill hole angles and groove hole angles is still lacking.

The performance of disc brakes is greatly influenced by material as well. The performance of disc brakes can be enhanced by choosing materials based on the appropriate material qualities. Shanker [21] asserted that the disc is a mechanical brake's most crucial component. The disc material needs to possess a high and repeatable coefficient of friction, environmental resilience, thermal stability, high wear resistance, flexibility, and compatibility with any surface. Vishvajeet et al. [22] have investigated the various disc brake materials and found that, when compared to carbon-carbon, aluminum, and titanium alloy, stainless steel provides the highest value of comparable stress. Additionally, it was shown that, compared to the other three materials,

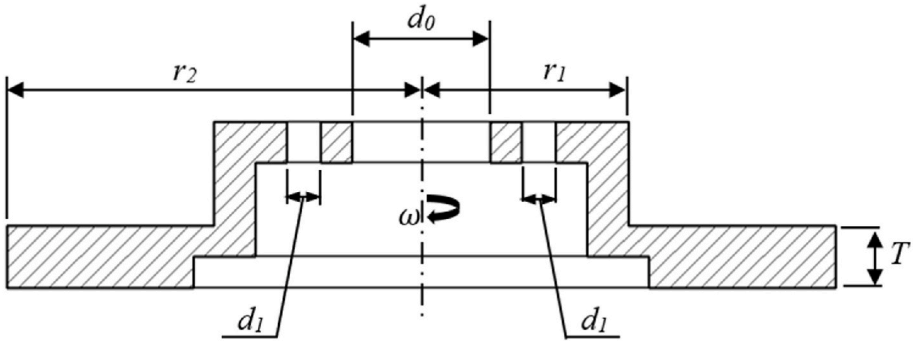

Fig. 2. Disc brake dimension.

Table 1
Disc brake geometry parameters.

Geometry Parameters	Symbol	Value	Units
Inner radius	r_1	60	mm
Outer radius	r_2	120	mm
Shaft diameter	d_0	40	mm
Wheel nut diameter	d_1	10	mm
Disc thickness	T	18	mm
Disc angular velocity	ω	300	rad/s

Table 2
The geometry parameters of isc brake drill type and groove type.

Parameter	Symbol	Value	Unit
Shaft diameter	d_0	40	mm
Wheel nut diameter	d_1	10	mm
Drill hole diameter	d_2	8	mm
Diameter of groove hole	g_1	5	mm
Arc length of groove hole	g_2	18.64	degree
Distance of drill hole 1 from shaft	L_1	74	mm
Distance of drill hole 2 from shaft	L_2	86	mm
Distance of drill hole 3 from shaft	L_3	98	mm
Distance of drill hole 4 from shaft	L_4	110	mm
Initial distance of groove hole to shaft	L_5	69	mm
Final distance of groove hole to shaft	L_6	115	mm
Inner radius	r_1	60	mm
Outer radius	r_2	120	mm
Disc thickness	T	18	mm
Distance of drill hole 2 to 1	α_1	3.04	degree
Distance drill hole 3 to 1	α_2	3.10	degree
Distance drill hole 4 to 1	α_3	3.18	degree
Ventilation hole angle	θ	0, 11, 22, 33, 44, 55	degree
Angular speed of the disc	ω	300	rad/s

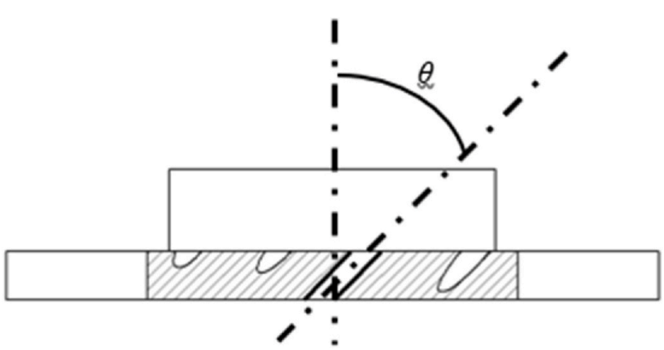

Fig. 3. Schematic of ventilation hole angle.

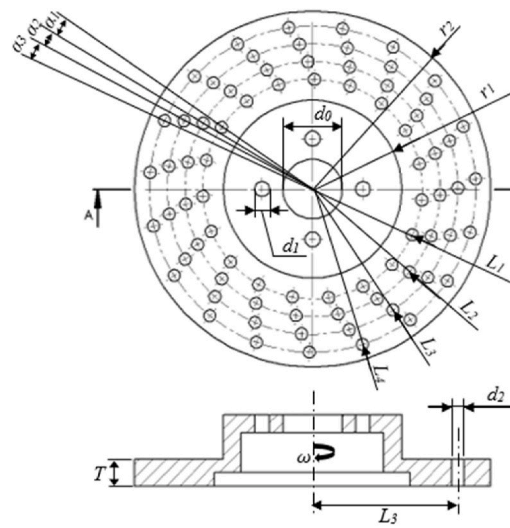

Fig. 4. Dimension of drill-type disc brake.

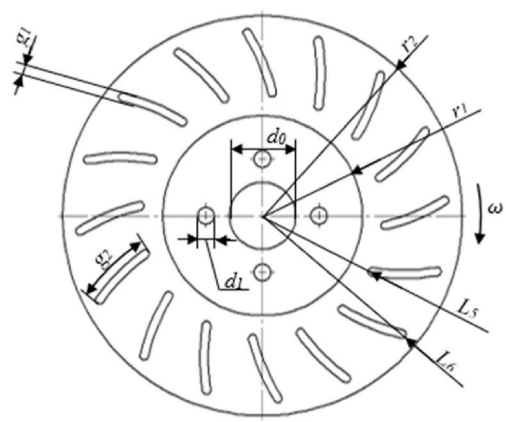

Fig. 5. Dimension of groove-type disc brake.

aluminum is the least effective at dissipating heat. Balaji et al. [23] investigated the tribological behavior of disk brake materials versus polymer composites. According to Maleque et al. [24], cast iron is the most frequently used material for disc rotors. However, after repeating the simulation with several materials, it was determined that lead and aluminum metal matrix composite may be employed as disc brake material. Mathad et al. [25] performed research to find a replacement of brake pad material with improved qualities that will prolong the life of the component. Materials considered include carbon ceramic and gray

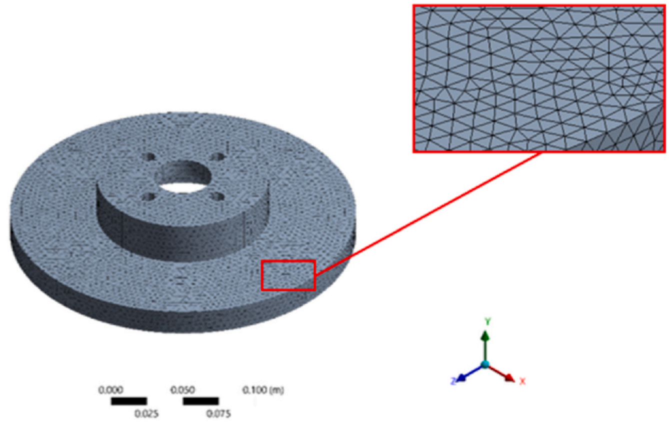

Fig. 6. Mesh of the disc brake.

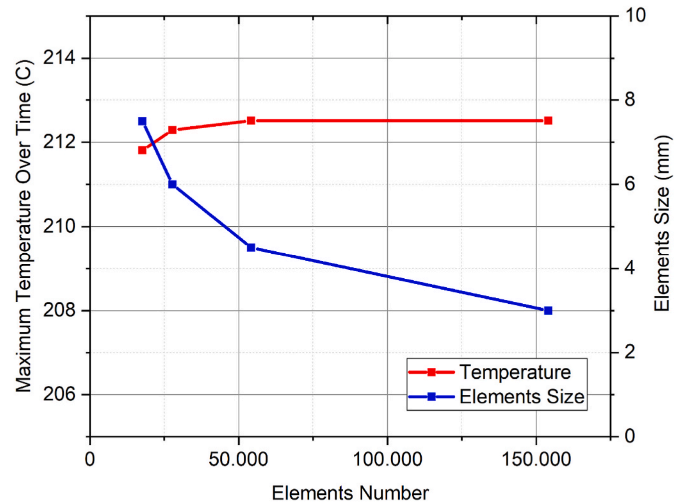

Fig. 7. Result of grid independency study.

Table 3
Meshing parameters.

Mesh Parameters	
Method	Tetrehedrons
Element size	4.5 mm
Number of elements	54,175
Number of nodes	350,014
Maximum skewness	0.66544
Minimum skewness	0.15212

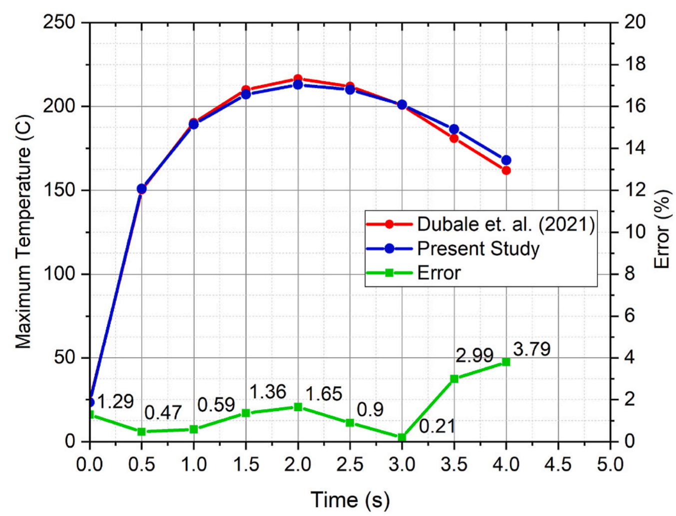

Fig. 8. Comparison of the maximum temperature vs time with results in reference (Dubale et al. [1]).

Table 4
Boundary conditions.

Boundary condition	Condition	Description
Convective heat transfer coefficient	230 W/m$^{2\circ}$C	All body
Initial temperature	22°C	All body

Table 5
Geometrical and mathematical properties.

Parameter	Material		
	Gray cast iron	Carbo ceramic	Stainless steel 420
Area of pad (m^2)	0.006136	0.006136	0.006136
Area disc	0.033921	0.033921	0.033921
Thermal effusivity ($Ws^{1/2}m^2K$)	13787.49	7589.47	9452.05
Partitioning coefficient	0.96	0.94	0.95
Heat flux	2.55×10^6 (1-t/4)	2.71×10^6 (1-t/4)	2.52×10^6 (1-t/4)

cast iron. Following validation, it was found that carbon ceramic disc brakes outperform the competition in terms of structural and thermal performance for the same boundary and loading conditions. Sau et al. [26] examined the various thermal properties of a material and how they change when applied to a car disc brake. The material was chosen to ensure long-term performance under the specified heat and friction conditions. By doing this, the reliance on driving characteristics to get the most out of brake rotors will be reduced. They have shown that stainless steel 420 demonstrated the best mechanical strength and heat dissipation rate under the chosen test conditions.

Based on the literature review above, it seems that there is no superior material of disc brake in improving heat dissipation. In order to complement previous findings on the disc brake material, it is necessary to conduct a distinct analysis, based on the finite element method, of the thermal property investigation of different types of disc brake (i.e. solid disc brake, drill-type disc brake, and groove-type disc brake) under different disc brake material types. Ventilation in disc brakes was proven to increase heat dissipation to the environment, according to the available studies that have been previously published. Creating ventilation holes at specific angles is also regarded as a novel and inventive technique, but no one has yet applied it to solid-type car disc brakes. Therefore, with this main framework, the novelty of the present work is a comprehensive comparative analysis, which has been imposed for the investigation of the effect of providing ventilation angles and varying material types on the thermal behavior of various types of car disc brakes.

2. Theory

In the braking process, friction between the brake disc and the pads converts the majority of the mechanical energy of a moving vehicle into heat. The heat energy is then released through the disc and the brake pads [27]. The friction during the braking process is incredibly intricate. All process variables (speed, load, temperature, and contact conditions) change over time while braking.

In the present work, the governing heat equations for discs are derived from the temporal-dependent heat equations [1]. In detail, due

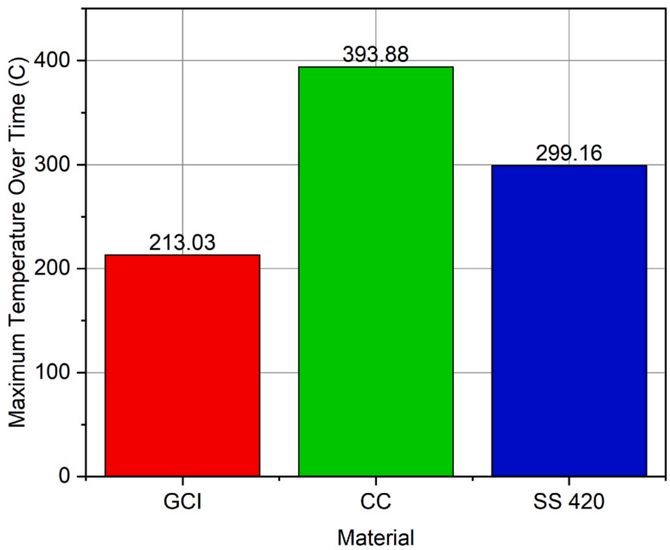

Fig. 9. Maximum temperature over time of solid-type disc brake for several materials. Note. GCI refers to gray cast iron, CC denotes carbon ceramic and SS 420 refers to stainless steel ASTM 420.

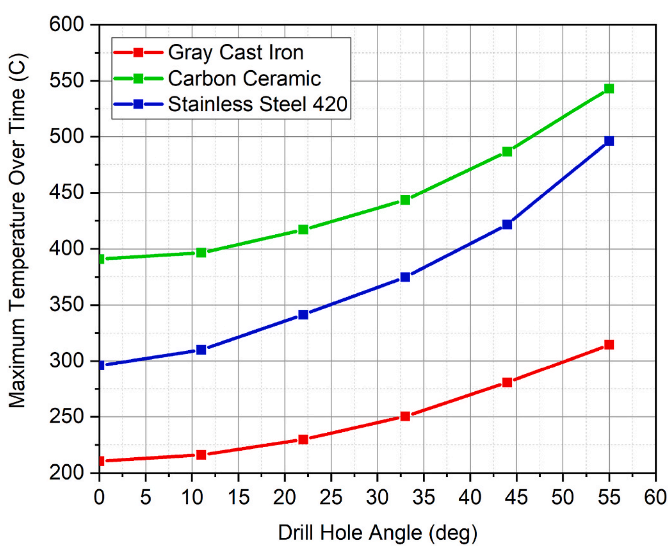

Fig. 10. Maximum temperature over time against drill hole angle.

to the thermodynamics of energy conservation through a solid being of particular interest, the governing equation for heat conduction through a solid is solved using the finite element method (FEM). In this study, the factors taken into account include contact pressure, vehicle speed, contact geometry parameters, and braking time. Therefore, analytical solutions to problems are proposed using the green function technique to complement the input for loading and boundary conditions of the computational domain of the disc brake during the simulation.

The purpose of this investigation is to identify the distribution of surface heat flow, frictional heat generation, pressure, temperature distribution with respect to braking time, radial temperature distribution on the surface, and stress thermal impacts. The following presumptions have been made:

1. All the kinetic energy on the surface of the disc brake is converted into frictional heat or heat flux.
2. Only conduction and convection are used in this analysis to transport heat.
3. Radiative heat transfer only accounts for 5%–10% of total heat transmission, making it insignificant.

3. Isotropic and temperature-independent material characteristics

The rate of heat generated by friction is equal to the frictional force; some of the heat is absorbed by the disc, and the remaining portion is absorbed by the bearing. It is assumed that all frictional energy is converted to heat energy and the parameters determine the heat partition coefficient. The brakes and bearings may receive heat energy generated at the brake friction interface. According to Dubale et al. [1], the heat partition coefficient can also be seen as a kind of relative braking energy. The partition coefficient is specified for the current analysis as [1]:

$$\varpi = \frac{\xi_d S_d}{\xi_d S_d + \xi_p S_p} \tag{1}$$

The frictional heat is divided across the contact surfaces in a shear contact with a high Peclet number, and it is greatly influenced by the geometry, thermo-physical characteristics of the contact material, and the contact conditions [28]. The thermal effusivity of the disc and pad are represented here by ξ_d and ξ_p. Material density, heat capacity, and thermal conductivity all influence thermal effusivity. The definition of thermal effusivity is [1]:

$$\xi = \sqrt{k\rho C_p} \tag{2}$$

A measure of a material's capacity to store and exchange thermal energy with its surroundings is provided by thermal effusion. It can be calculated as the square root of the thermal conductivity, density, and specific heat product [29]. Calculated as follows, S_p and S_d are the friction contact surfaces of the pad and disc, respectively [1]:

$$S_p = \varphi_0 \int_{r_1}^{r_2} r dr \tag{3}$$

$$S_d = 2\pi \int_{r_1}^{r_2} r dr \tag{4}$$

The microplastic deformation caused by the frictional force during braking is what causes the heat between the pad and the disc's contact region. Heating refers to the manifestation of the conversion of mechanical energy into heat energy. To calculate the heat flow in the brake system component, divide the rate of heat energy by the surface contact area of the component [30]. Disc and pad surfaces come into touch. The following formula is used to calculate how much heat is produced by friction between various surfaces [1]:

$$d\dot{E} = dp = VdF_f = r\omega\mu p\varphi_0 r dr \tag{5a}$$

$$d\dot{E} = d\dot{E}_p + d\dot{E}_d \tag{5b}$$

$$d\dot{E}_p = (1-\varpi)dp = (1-\varpi)\omega\mu p\varphi_0 r^2 dr \tag{5c}$$

$$d\dot{E}_d = \varpi dp = \varpi\omega\mu p\varphi_0 r^2 dr \tag{5d}$$

where V is the relative shear velocity, dF_f is the frictional force which is a function of the friction coefficient, and $d\dot{E}$ is the rate at which heat is produced as a result of friction between two components that are in shear contact. The coefficient of friction is calculated by multiplying the applied normal load by the observed tangential force [31]. The quantity of heat absorbed by the pad and disc, respectively, is indicated by the symbols $d\dot{E}_p$ and $d\dot{E}_d$.

Rate of heat energy divided by each component's surface contact area reads:

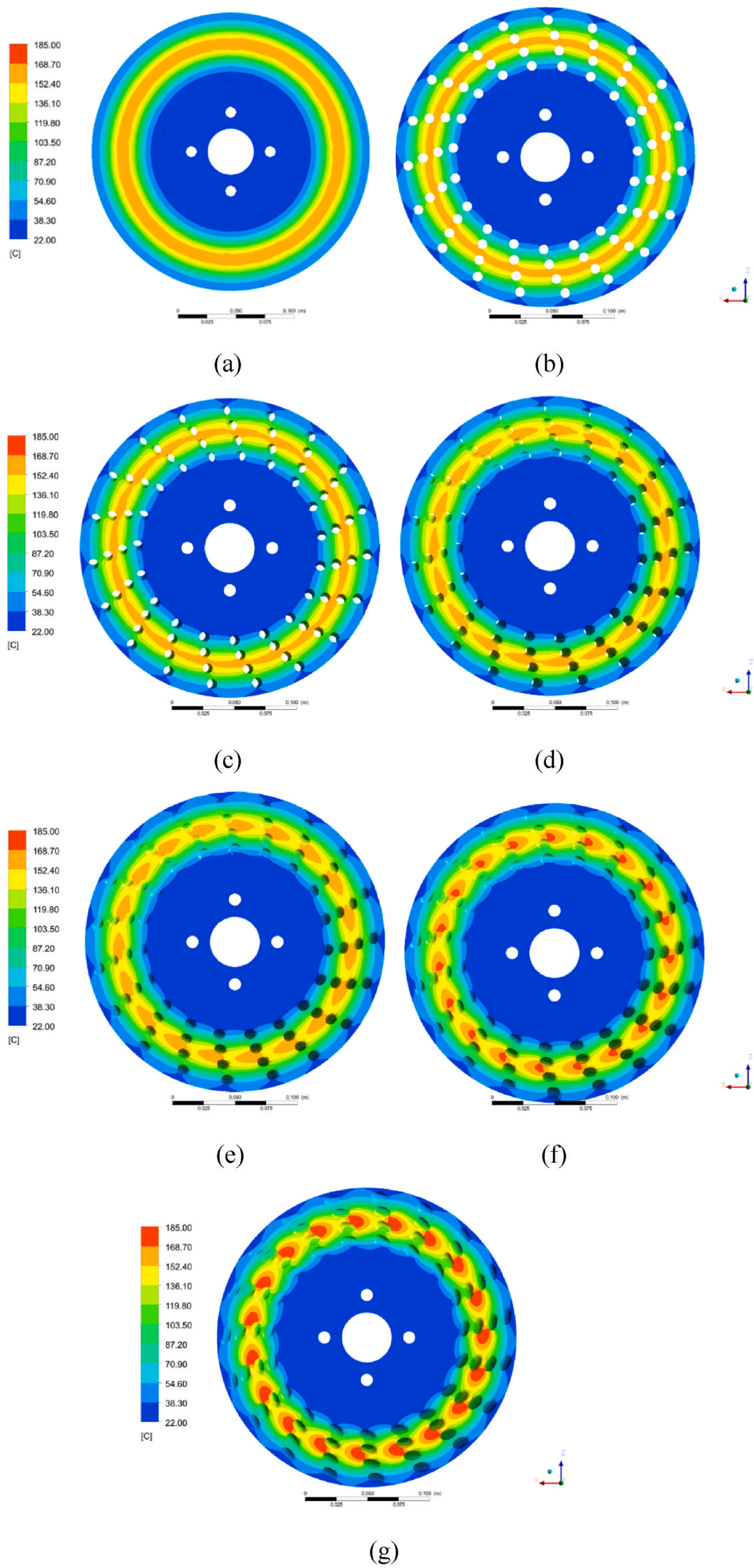

Fig. 11. Temperature distribution of disc brake with gray cast iron material for the case of (a) solid type, (b) drill type with $\theta = 0°$, (c) drill type with $\theta = 11°$, (d) drill type with $\theta = 22°$, (e) drill type with $\theta = 33°$, (f) drill type with $\theta = 44°$, and (g) drill type with $\theta = 55°$.

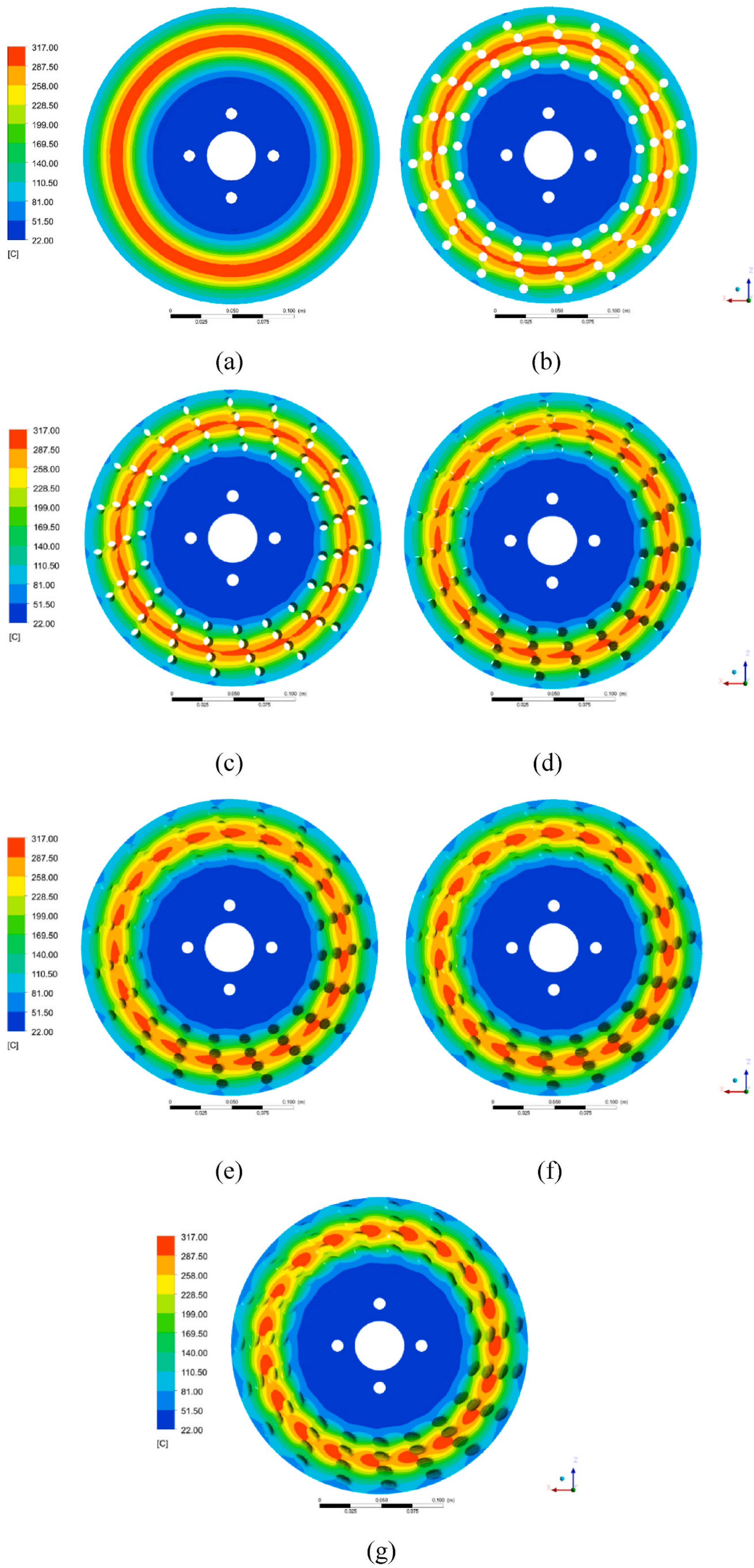

Fig. 12. Temperature distribution of disc brake with carbon ceramic material for the case of (a) solid type, (b) drill type with $\theta = 0^\circ$, (c) drill type with $\theta = 11^\circ$, (d) drill type with $\theta = 22^\circ$, (e) drill type with $\theta = 33^\circ$, (f) drill type with $\theta = 44^\circ$, and (g) drill type with $\theta = 55^\circ$.

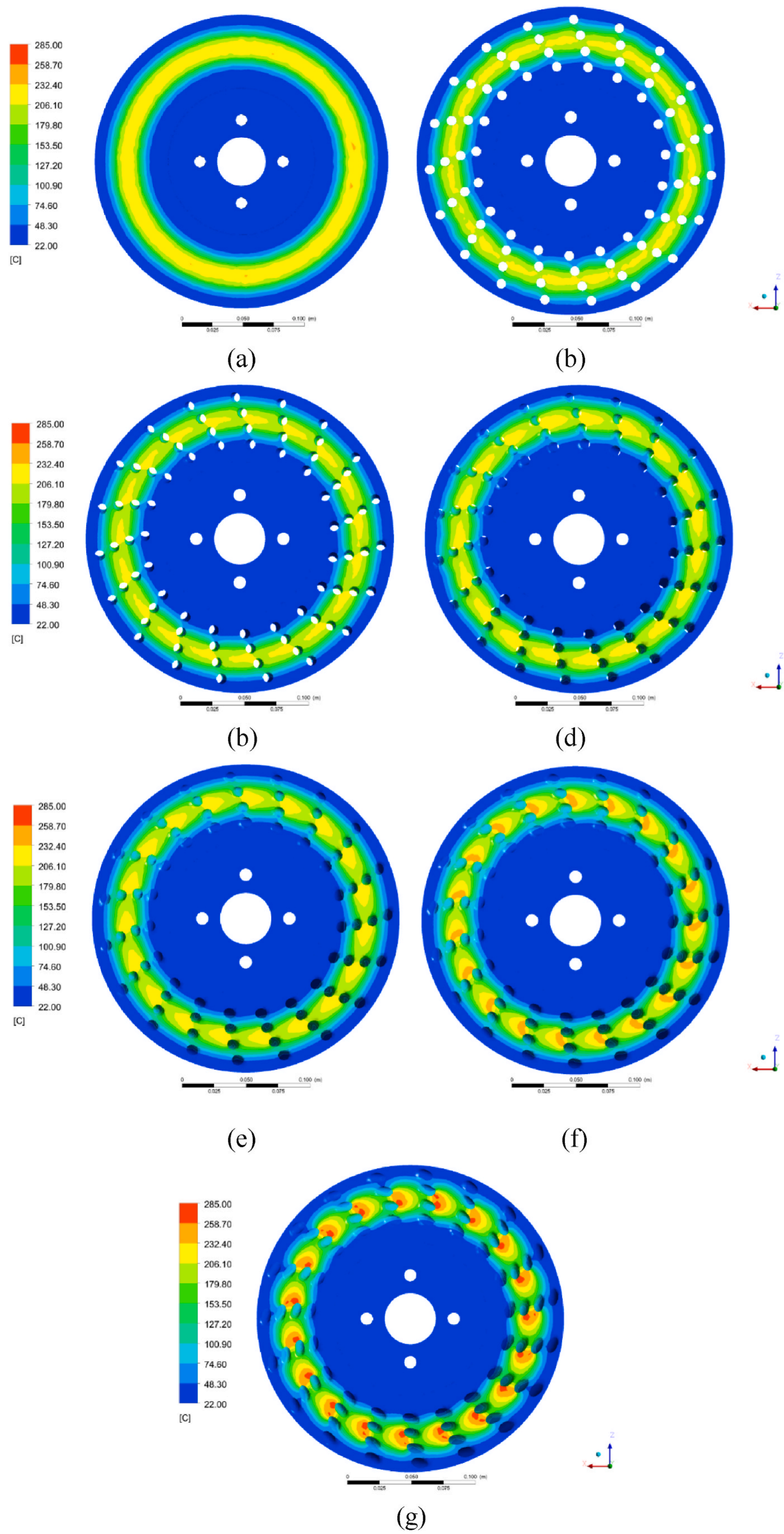

Fig. 13. Temperature distribution of disc brake with stainless steel ASTM 420 material for the case of (a) solid type, (b) drill type with $\theta = 0°$, (c) drill type with $\theta = 11°$, (d) drill type with $\theta = 22°$, (e) drill type with $\theta = 33°$, (f) drill type with $\theta = 44°$, and (g) drill type with $\theta = 55°$.

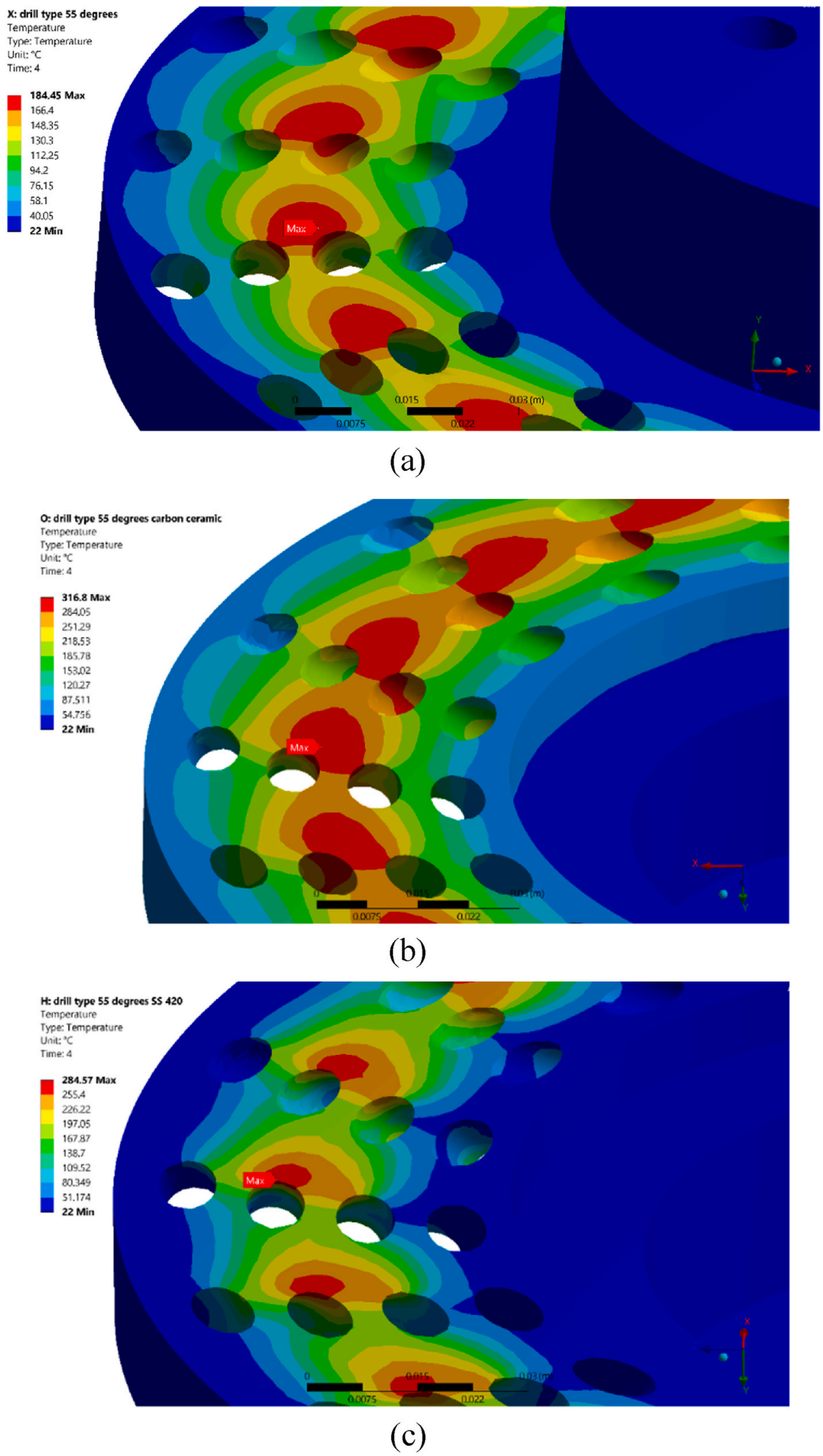

Fig. 14. Temperature distribution of drill-type disc brake with $\theta = 55^{\circ}$ for the material of (a) gray cast iron, (b) carbon ceramic, (c) stainless steel ASTM 420.

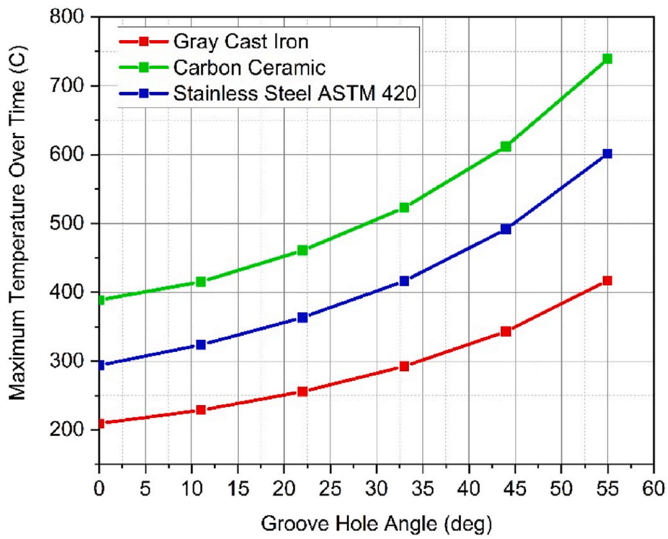

Fig. 15. Maximum temperature over time against groove hole angle.

3.1. Heat flux for pad

$$q_1(r,t)=\frac{d\dot{E}_p}{dS_p}=(1-\varpi)\mu p(t)r\omega(t) \tag{6a}$$

$$q_{0_1}(r)=q_1(r,0)=(1-\varpi)\mu\, pr\,\omega_0 \tag{6b}$$

when entered $p=P_{\max}\frac{r_3}{r}$ into Equation (6a), the result is,

$$q_1(r,t)=\frac{d\dot{E}_p}{dS_p}=(1-\varpi)\mu P_{\max}r_3\omega_0\left(1-\frac{t}{t_b}\right) \tag{6c}$$

3.2. Heat flux for disc

$$q_2(r,t)=\frac{d\dot{E}_d}{dS_d}=\frac{\varphi_0}{2\pi}\mu\varpi p(t)r\omega(t) \tag{7a}$$

$$q_{0_2}(r)=q_{0_2}(r,0)=\frac{\varphi_0}{2\pi}\mu\varpi\, pr\,\omega_0 \tag{7b}$$

When entered $p=P_{\max}\frac{r_3}{r}$ into Equation (6a), the result is,

$$q_2(r,t)=q_{0_2}(r)*\left(1-\frac{t}{t_b}\right)=\frac{\varphi_0}{2\pi}\mu\varpi P_{\max}r_3\omega_0 \tag{7c}$$

4. Materials and methods

4.1. Geometry

The geometry of the disc brake model employed here is inspired by disc brake geometry from Dubale et al. [1]. Based on this geometry, the drill-type and the groove-type disc brakes are proposed. Figs. 1 and 2 below show the nomenclature and basic geometry of the disc brake model. In detail, the dimensional parameters of the disc brake are presented in Table 1. For drill-type and groove-type disc brakes, the geometry parameters are shown in Table 2.

The basic geometry is the solid type geometry from Dubale et al. [1], and the drill hole and groove hole angle are provided as a variant. The distribution of drill and groove hole angle variations is based on research published by Choudhary et al. [20]. Here, ventilation hole angles of 0°, 11°, 22°, 33°, 44°, and 55° are of particular interest. Giving angles greater than 55° is impossible due to the presence of tangents. However, a drill hole slope and a groove hole inserted into the disc brake surface contribute geometry to the angle. Figs. 3–5 below show the specifics of the schematic drawings for the disc brake of drill type and groove type.

4.2. Meshing

In this study, for the simulation, the tetrahedrons method is employed throughout the meshing process to create a reasonably effective mesh. As discussed by Oberst and his/her group [32,33], the tetrahedral element has the advantage of being compatible with the majority of meshing techniques when it comes to complex constructions with more realistic geometry such as disc brakes. To gauge how good the final mesh is, mesh quality control is introduced. This quality check uses the skewness method to evaluate how well the mesh performs. How closely a face or cell resembles the ideal shape (i.e., equilateral or equiangular) is determined by its skewness. Fig. 6 and Table 3 below provide a detailed look at the mesh configuration and the mesh formation criteria. In Table 3, it can be seen that the maximum skewness is 0.66 which is still in the good category. All simulations also use elementsize of 4.5 mm because it offers a respectable amount of independent mesh and a tolerable computation time.

4.3. Boundary conditions

The boundary condition employed here adopts the simulation by Dubale et al. [1]. Table 4 details the boundary condition used in all subsequent simulations. It should be noted that the analytical results of mathematical modeling in the form of a function become the computational domain loading for numerical simulation.

Table 5 provides a summary of the loading inputs based on the analytical calculation of the mathematical modeling. The value of $q_2(t)$, which is the amount of heat absorbed by the disc brake, is determined from the mathematical modeling. This value depends on (1) the material utilized as an input for transient analysis, which in ANSYS is modeled as heat flux, and (2) time. Because the value is so low, the area difference resulting from geometric variance is ignored.

4.4. Grid independency test

All of the computational models in this study are based on three-dimensional physical models of discs. To ensure the accuracy of the results, the sensitivity of grid density to temperature is checked for the computational domain. The refinement criteria, that is, the element size with linear proportion, is specified to achieve satisfactory convergence. Each computation is performed using a different element number under the same operating conditions. Fig. 7 depicts the results of the grid-independent study in terms of maximum temperature over time for various element number and element size combinations. According to Fig. 7, the element size is determined after sensitivity analysis reveals that several element size values change the maximum temperature of the disc over time by less than 2% in the finite element model. To summarize, the computational domain element size of 4.5 mm, as shown in Fig. 7, is used for all simulations because it provides a reasonable computational time with a feasible level of independent mesh.

5. Results and discussion

5.1. Validation

To demonstrate that the present computational method and solution setup can be used for thermal analysis of the disc brake, it must be revealed that the results are correct and with specified accuracy in the numerical framework. The developed finite element model is validated in this section. Computations were performed by comparing the results of this study to those of Dubale et al. [1] under the same working conditions. The correlation between the maximum temperature and time is depicted in Fig. 8. Observe that the obtained values from the finite element method (FEM) developed here are extremely close to the

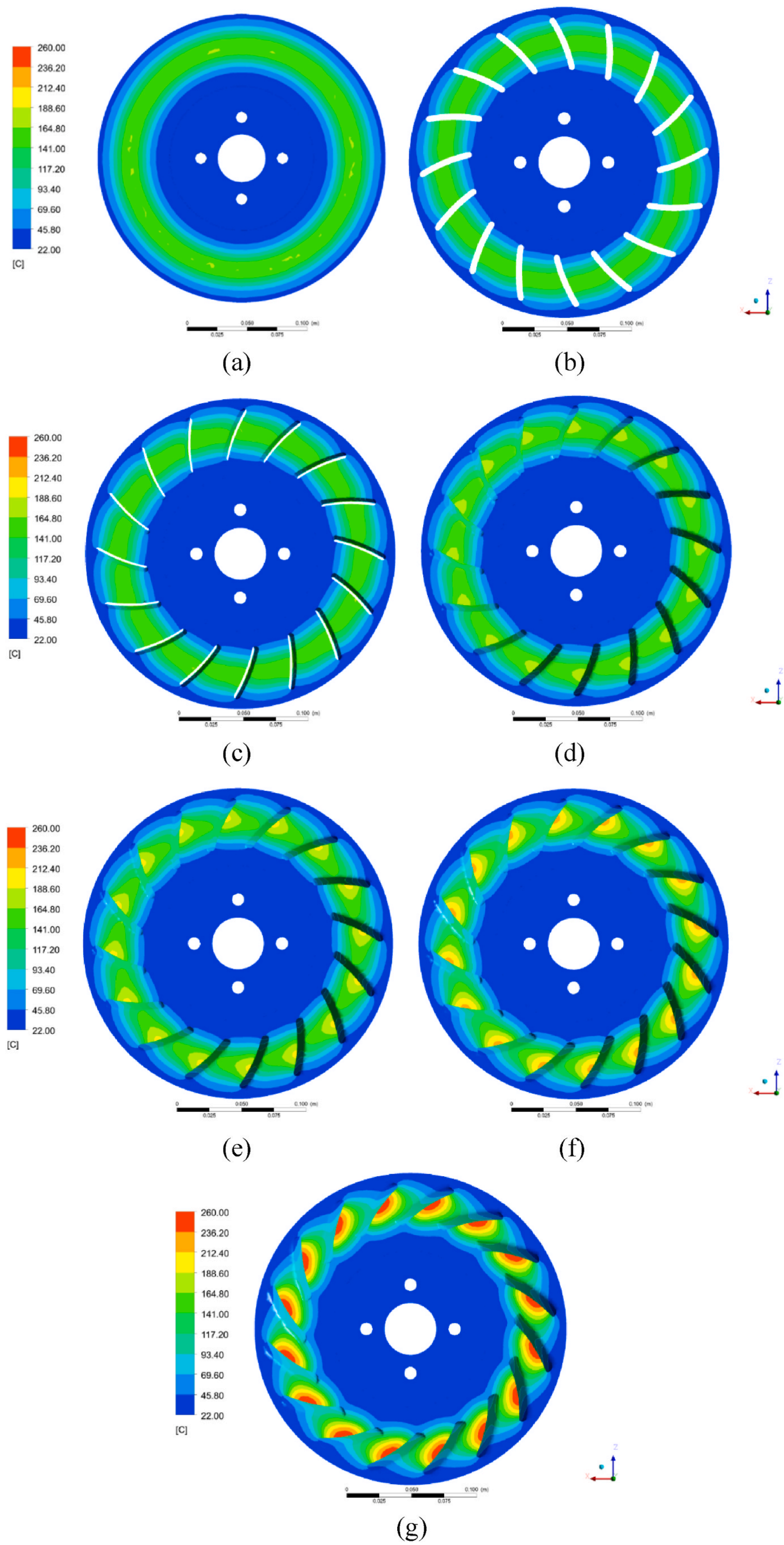

Fig. 16. Temperature distribution of disc brake with gray cast iron material for the case of (a) solid type, (b) groove type with $\theta = 0^{\circ}$, (c) groove type with $\theta = 11^{\circ}$, (d) groove type with $\theta = 22^{\circ}$, (e) groove type with $\theta = 33^{\circ}$, (f) groove type with $\theta = 44^{\circ}$, and (g) groove type with $\theta = 55^{\circ}$.

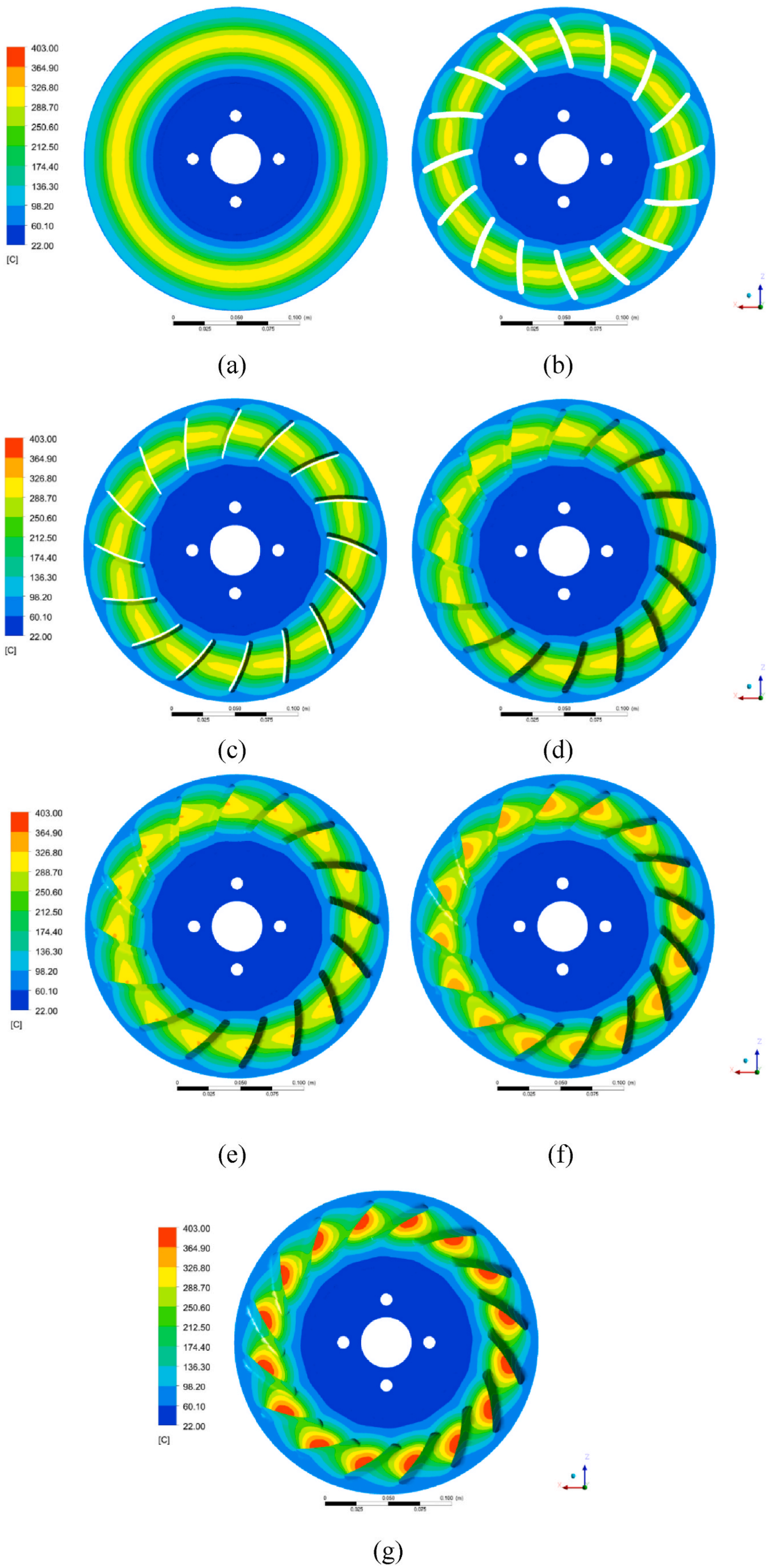

Fig. 17. Temperature distribution of disc brake with carbon ceramic material for the case of (a) solid type, (b) groove type with $\theta = 0^\circ$, (c) groove type with $\theta = 11^\circ$, (d) groove type with $\theta = 22^\circ$, (e) groove type with $\theta = 33^\circ$, (f) groove type with $\theta = 44^\circ$, and (g) groove type with $\theta = 55^\circ$.

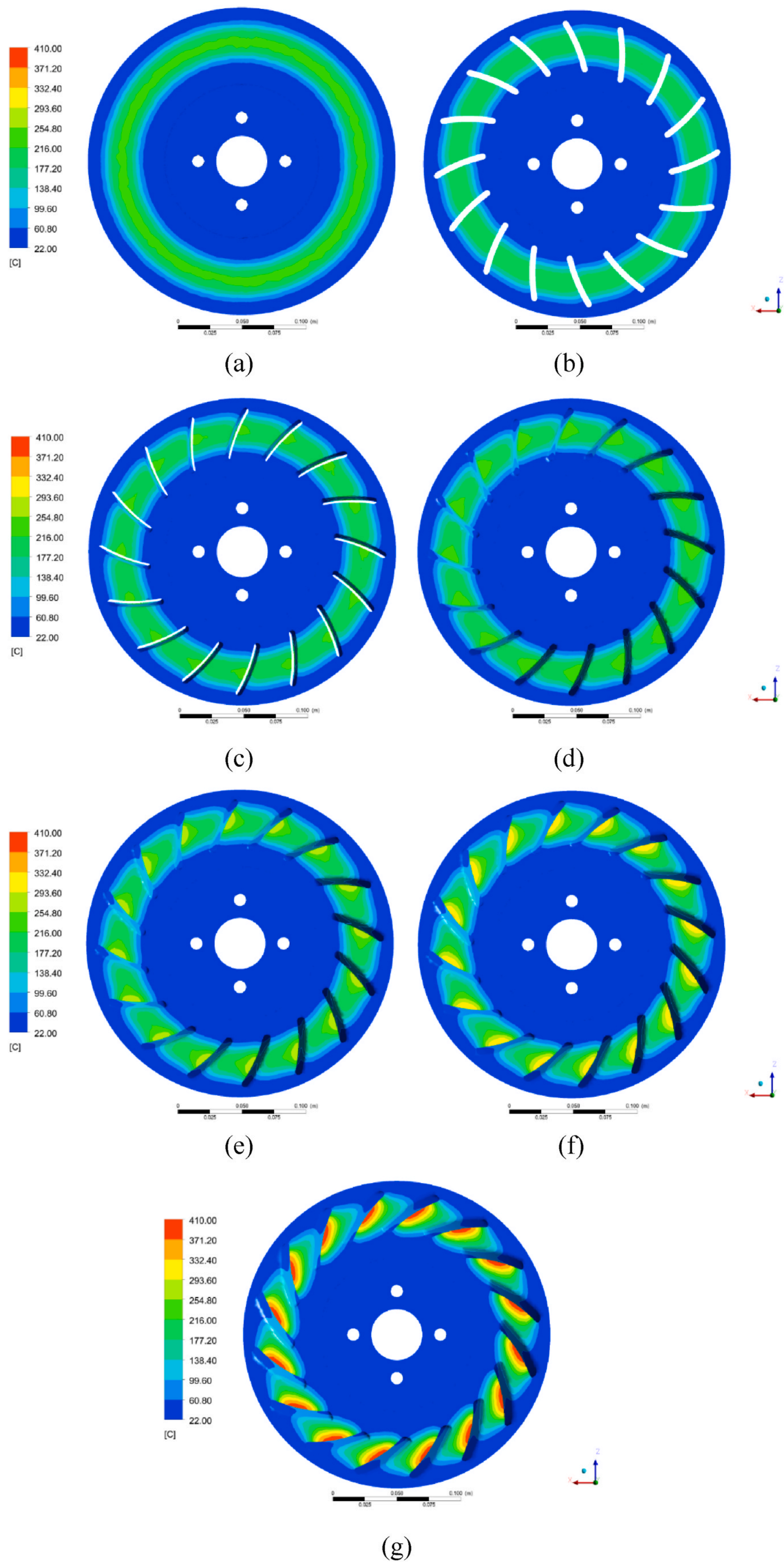

Fig. 18. Temperature distribution of disc brake with stainless steel ASTM 420 material for the case of (a) solid type, (b) groove type with $\theta = 0^{\circ}$, (c) groove type with $\theta = 11^{\circ}$, (d) groove type with $\theta = 22^{\circ}$, (e) groove type with $\theta = 33^{\circ}$, (f) groove type with $\theta = 44^{\circ}$, and (g) groove type with $\theta = 55^{\circ}$.

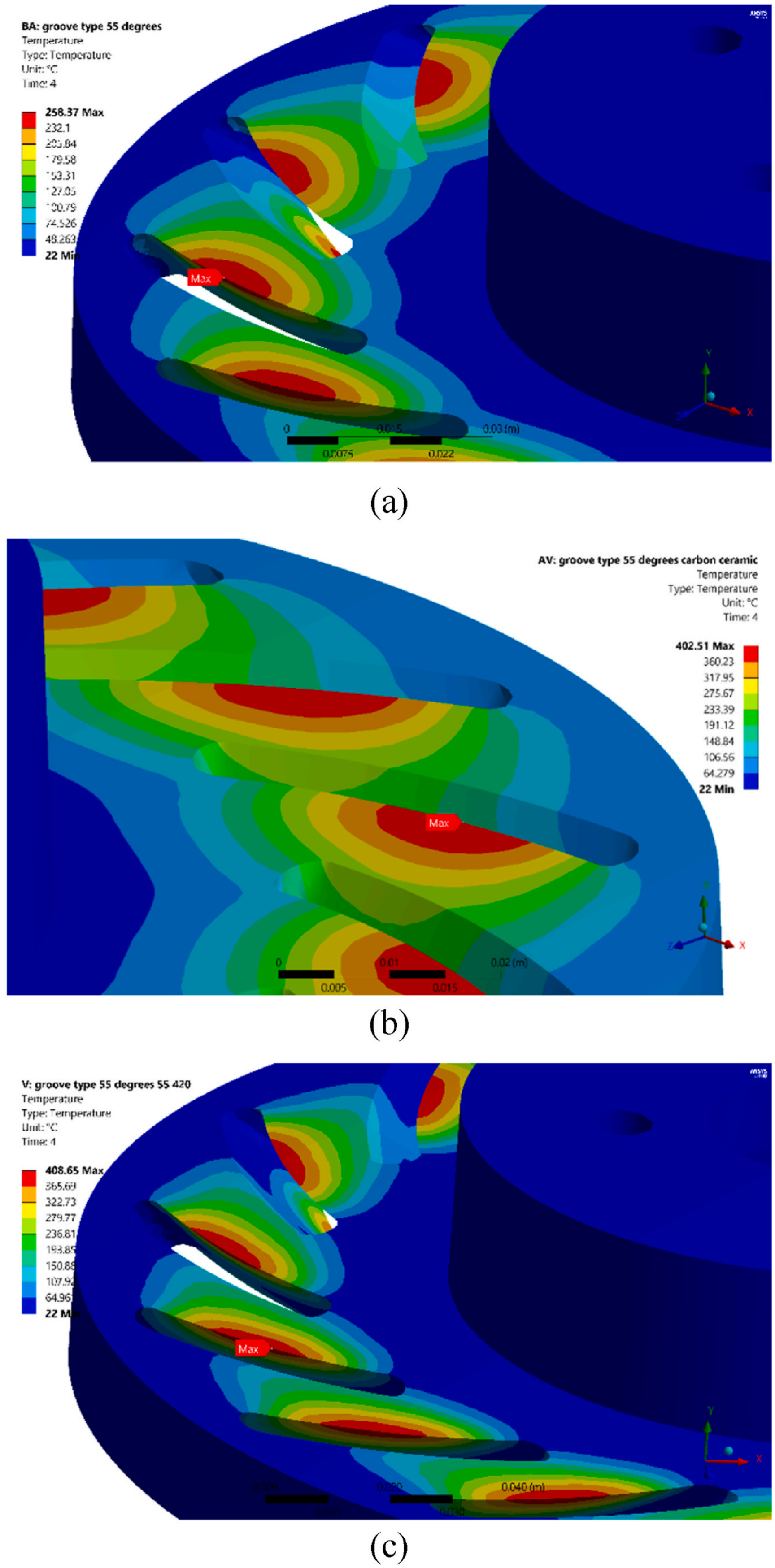

Fig. 19. Temperature distribution of groove-type brake with $\theta = 55^{\circ}$ for the material of (a) gray cast iron, (b) carbon ceramic, (c) stainless steel ASTM 420.

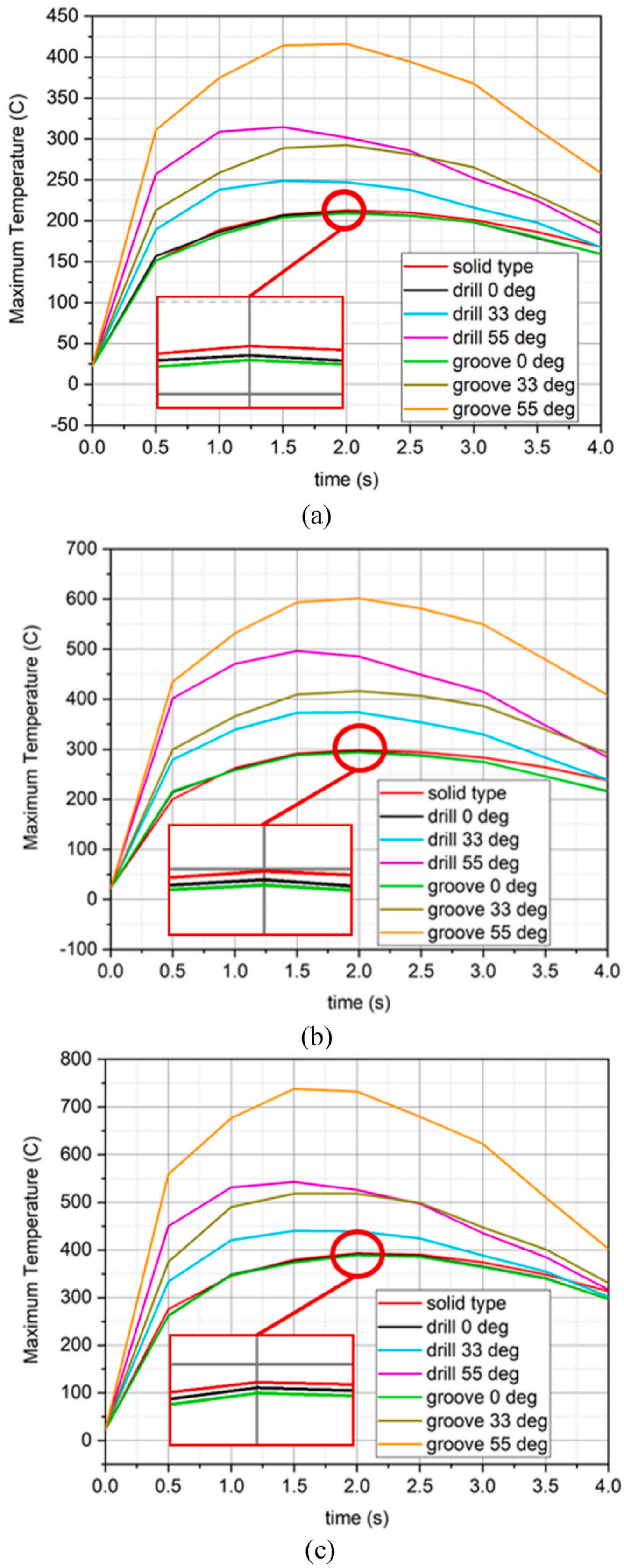

Fig. 20. Comparison of thermal performance for several materials, (a) gray cast iron, (b) stainless steel ASTM 420, (c) carbon ceramic.

numerical results previously published. Moreover, as shown in Fig. 8, their differences are all less than 4%. In general, the FEM code, which incorporates the analytical solution, has been shown to accurately simulate the thermal behavior inside the disc brake.

5.2. Case of solid-type disc brake

In this section, the objective is to explore the thermal characteristic of the case of solid-type disc brakes varying the material types. Using ANSYS transient thermal, the data was produced in terms of the highest temperature over time and temperature distribution contours. Fig. 9 depicts the maximum temperature over time for several solid-type disc brake materials, including gray cast iron, carbon ceramic, and stainless steel ASTM 420. Fig. 9 indicates that the carbon ceramic disc brake, with a maximum temperature of 393.88 °C, has the highest maximum temperature over time. A solid-type disc brake with gray cast iron material has a maximum temperature value over time of 213.03 °C, while a solid-type disc brake with stainless steel ASTM 420 material has a maximum temperature value over time of 299.16 °C.

Furthermore, based on Fig. 9, it can be revealed that since gray cast iron has the lowest maximum temperature (213.03 °C), and thus, it can be regarded as the ideal material for disc brakes. Due to high thermal conductivity, brake disc made of cast iron is more efficient at dissipating heat, but its heavier weight is a disadvantage [34]. Thermal effusion, in addition to thermal conductivity, has a significant impact on the maximum temperature. Because of its low thermal effusion value, carbon ceramic has the highest maximum temperature value. According to the research conducted by Cartigny et al. [35], the use of materials with a high thermal effusion increases the flow produced at the interface that is conveyed to the brake, thereby reducing the surface temperature.

5.3. Case of drill-type disc brake

As is well known, the theoretical foundation states that the area of the disc brakes increases as the drill angle increases. According to Newton's equation of cooling, the amount of heat that can be transferred to the environment grows as the area does as well. The disc brake's temperature is projected to drop as a result of this theory. To incorporate this issue, the maximum temperature over time against drill hole angle is shown in Fig. 10. However, an interesting finding is observed based on Fig. 10. As the drill angle increases, the maximum temperature tends to rise over time. The same trend was observed with many different kinds of materials. This runs contrary to the premise that was presented earlier. After a more thorough investigation, it can be seen that changing the drill angle resulted in both an increase in the heat release area and a decrease in the thickness of the disc at various locations. The decrease in disc thickness is what causes the maximum temperature to rise over time. Based on the work of Newcomb [36], it was shown that as disc thickness decreases, the maximum surface temperature climbs noticeably.

Figs. 11–13 show a concentration of heat at various locations. All materials experience convergence. Solid-type discs and drill-type discs with $\theta = 0^\circ$ do not experience this heat concentration. On the drill type disc with $\theta = 11^\circ$, however, it begins to center and focus more as the angle rises. The temperature at that point tends to rise with the addition of the drill angle in addition to the increasingly concentrated temperature point. Fig. 14 illustrates the temperature contour of drill-type of disc brake with $\theta = 55^\circ$ for all materials considered here. Due to the angle of the drill type, there is a concentration of heat on the disc, whose thickness decreases. This point has the highest temperature value in the entire area.

5.4. Case of groove-type disc brake

The simulation results of brake modifications varying the groove angle for several materials of the groove-type disc brake in terms of thermal performance are presented in this section. Here, the maximum temperature over time and temperature distribution are of particular interest. As can be seen in Fig. 15, the maximum temperature rises in tandem with an increase in the groove hole angle. This trend exhibits the same phenomenon as the drill hole angle trend. The most possible explanation is that increasing the groove hole angle will cause a thinning of the geometry of the disc brake. To strengthen this finding, the temperature distributions for all materials with different hole (or groove) angles are presented in Figs. 16–18, while heat concentration can be seen in Fig. 19. It can be observed in Figs. 16–19, that for all materials considered here, the maximum temperature increases with increasing the ventilation hole angle. Heat concentration occurs in regions of geometric depletion, specifically in the region closest to the ventilation holes.

5.5. At varied types of material

To investigate the thermal characteristics of a variety of disc brake types, as discussed in the previous section, it is necessary to summarize the effect of ventilation hole angle for all of the materials considered here. Here, on various materials, the simulation results for each geometry are compared. As observed in Fig. 20, the correlation between maximum temperature and time for each material is presented. Based on Fig. 20, it can be highlighted that concerning maximum temperature, groove-type disc brake with ventilation hole angle θ of 0° has the lowest value. This is slightly different from the maximum temperature value in the case of the solid-type disc brake and the drill-type disc brake with the same θ. The present results are in good agreement with the work of Dubale et al. [1], who stated that the groove-type disc brake with $\theta = 0^\circ$ has the lowest maximum temperature value. The addition of angle variations in the drill hole and groove hole results in a rise in the maximum temperature value.

6. Conclusion

In this study, a finite element analysis is performed to evaluate the thermal behavior of three types of disc brakes including solid type, groove type, and drill type. Furthermore, the effect of ventilation hole angle modification on the thermal performance of a particular disc brake made from different materials (i.e. gray cast iron, carbon ceramic, and stainless steel ASTM 420) was also discussed. From the numerical results, the following conclusions can be drawn:

1. Variations in the drill hole angle and groove hole angle for the three types of disc brake studied here show that the groove-type disc brake with a ventilation hole angle of 0° has the best thermal performance, i.e. the lowest maximum temperature.
2. The maximum temperature value of the disc brake is increased by the addition of the drill hole angle and groove hole angle. Certain regions experience heat concentration as a result of geometry thinning.
3. The increase in the maximum temperature value along with the addition of the drill hole angle and groove hole angle occurs in all disc brake materials (i.e. cast gray iron, stainless steel 420, and carbon ceramic). Nevertheless, gray cast iron has the smallest maximum temperature value due to the value of thermal effusivity.

Author contributions

Mohammad Tauviqirrahman: Conceptualization, funding acquisition, writing-review & editing, investigation. **Budi Setyana:** Data curation, visualization, software. **Muchammad:** Project administration, methodology. **Tian Setiazi**: Original draft preparation, resources. **Jamari**; Supervision, formal analysis, All authors have read and agreed to the published version of the manuscript.

Funding

This research is fully funded by RPI Grant, No. 233–29/UN7.6.1/PP/2020.

Declaration of competing interest

The authors declare that they have no known competing financial interests or personal relationships that could have appeared to influence the work reported in this paper.

Data availability

Data will be made available on request.

Acknowledgments

The authors fully acknowledged to Institute for Research and Community Services (LPPM) - Diponegoro University, Indonesia for the approved fund which makes this important research viable and effective.

References

[1] H. Dubale, V. Paramasivam, E. Gardie, E.T. Chekol, S.K. Selvaraj, Numerical investigation of thermo-mechanical properties for disc brake using light commercial vehicle, Mater. Today Proc. 46 (2021) 7548–7555, https://doi.org/10.1016/j.matpr.2021.01.437.
[2] R.A. García-León, N. Afanador-García, J.A. Gómez-Camperos, Numerical study of heat transfer and speed air flow on performance of an auto-ventilated disc brake, Fluid 6 (4) (2021) 160, https://doi.org/10.3390/fluids6040160.
[3] Bc Goo, Ch Lim, Thermal fatigue of cast iron brake disk materials, Journal Mechchanical Science Technology 26 (2012) 1719–1724, https://doi.org/10.1007/s12206-012-0435-2, 10.1007/s12206-012-0435-2.
[4] M.D. Didier, P. Dufrenoy, Y. Berthier, Tribological, thermal and mechanical coupling aspects of the dry sliding contact, Tribol. Int. 40 (5) (2007) 834–843, https://doi.org/10.1016/j.triboint.2006.08.004.
[5] M. Tirovic, G. Ali, Design synthesis of non-symmetrically loaded high-performance disc brakes Part 1, Proc. Inst. Mech. Eng. - Part F J. Rail Rapid Transit 215 (2) (2001) 101–109, https://doi.org/10.1243/0954409011531431.
[6] F. Talati, S. Jalalifar, Analysis of heat conduction in disk brake system, Heat Mass Tran. 45 (2009) 1047–1059, https://doi.org/10.1007/s00231-009-0476-y.
[7] M.R. Eslami, R.B. Hetnarski, N. Noda, J. Ignaczak, N. Sumi, Y. Tanigawa, Theory of Elasticity and Thermal Stresses vol. 197, Springer, Dordrecht, 2013, https://doi.org/10.1080/01495739.2013.846763.
[8] M.K. Khalid, M.R. Mansor, S.A. Kudus, M.M. Tahir, M.Z. Hassan, Performance investigation of the UTeM eco-car disc brake system, Int. J. Eng. Technol. 11 (6) (2011) 1–6.
[9] A. Belhocine, M. Bouchetara, Thermal analysis of a solid brake disc, Appl. Therm. Eng. 32 (2012) 59–67, https://doi.org/10.1016/j.applthermaleng.2011.08.029.
[10] C. Pinca-Bretotean, et al., An investigation of thermal behaviour of brake disk pad assembly with Ansys, Mater. Today Proc. 47 (2021) 2322–2328, https://doi.org/10.1016/j.matpr.2021.04.296.
[11] J. Bijwe, Nidhi, N. Majumdar, B. Satapathy, Influence of modified phenolic resins on the fade and recovery behavior of friction materials, Wear 259 (7–12) (2005) 1068–1078, https://doi.org/10.1016/j.wear.2005.01.011.
[12] A. Day, Braking of Road Vehicles, Butterworth-Heinemann, Oxford, 2014, pp. 215–258.
[13] X. Nong, Y. Jiang, M. Fang, L. Yu, C. Liu, Numerical analysis of novel SiC3D/Al alloy co-continuous composites ventilated brake disc, Int. J. Heat Mass Tran. 108 (2017) 1374–1382, https://doi.org/10.1016/j.ijheatmasstransfer.2016.11.108.
[14] H. Yan, W. Wu, S. Feng, G. Xie, Role of vane configuration on the heat dissipation performance of ventilated brake discs, Appl. Therm. Eng. 136 (2018) 118–130, https://doi.org/10.1016/j.applthermaleng.2018.03.002.
[15] A. Vdovin, M. Gustafsson, S. Sebben, A coupled approach for vehicle brake cooling performance simulations, Int. J. Therm. Sci. 132 (2018) 257–266, https://doi.org/10.1016/j.ijthermalsci.2018.05.016.
[16] A. Belhocine, M. Bouchetara, Thermomechanical modelling of dry contacts in automotive disc brake, Int. J. Therm. Sci. 1 (2012) 161–170, https://doi.org/10.1016/j.ijthermalsci.2012.05.006.
[17] S. Sarkar, P.P. Rathod, Review paper on thermal analysis of ventilated disc brake by varying design parameters, Int. J. Eng. Res. Technol. 2 (2013) 2278, https://doi.org/10.17577/IJERTV2IS120586, 0181.
[18] D.K. Dhir, Thermo-mechanical performance of automotive disc brakes, Mater. Today Proc. 5 (2018) 1864–1871, https://doi.org/10.1016/j.matpr.2017.11.287.
[19] J. Gerlici, Y. Fomina, K. Kravchenko, The dependence of the brake disc aerodynamic drag on the rolling stock motion speed, Transport. Res. Procedia 55 (2021) 723–730, https://doi.org/10.1016/j.trpro.2021.07.174.

[20] A. Choudhary, A. Jaiswal, A. Kant, M. Zunaid, N.A. Ansari, Coupled thermal and structural analysis of disc brake rotor with varying angle of rotation of ventilation holes, Mater. Today Proc. 56 (2022) 834–844, https://doi.org/10.1016/j.matpr.2022.02.490.
[21] P.S. Shanker, A review on properties of conventional and metal matrix composite materials in manufacturing of disc brake, Mater. Today Proc. 5 (2) (2018) 5864–5869, https://doi.org/10.1016/j.matpr.2017.12.184.
[22] Vishvajeet, F. Ahmad, M. Sethi, R.K. Tripathi, Thermo-mechanical analysis of disk brake using finite element analysis, Mater. Today Proc. (2021) 2214–7853, https://doi.org/10.1016/j.matpr.2021.04.614.
[23] R. Balaji, M. Nadarajan, A. Selokar, S.S. Kumar, S. Sivakumar, Modelling and analysis of disk brake under tribological behaviour of Al-Al2O3 ceramic matrix composites/Kevlar 119 composite/C/Sic-carbon matrix composite/Cr-Ni-Mo-V steel, Mater. Today Proc. 1 (2019) 3415–3427, https://doi.org/10.1016/j.matpr.2019.07.269.
[24] M.A. Maleque, S. Dyuti, M.M. Rahman, in: Procees of the World Congress on Engineering, Material selection method in design of automotive brake disc, London, UK, 2010.
[25] M. Mathad, et al., Non-Linear structural and thermal analysis of automotive brake disc, Mater. Today Proc. 59 (2022) 1221–1224, https://doi.org/10.1016/j.matpr.2022.03.426.
[26] S.K. Sau, G.K. Pulinat, N.P. Moss, P. Ranjeet, S.S. Prabu, A comparative study on the thermal and dynamic analysis of a disc brake using Ansys, Mater. Today Proc. 65 (2022) 3714–3723, https://doi.org/10.1016/j.matpr.2022.06.318.
[27] A. Belhocine, M. Bouchetara, Structural and thermal analysis of automotive disc brake rotor, Arch. Mech. Eng. 61 (1) (2014), https://doi.org/10.2478/meceng-2014-0005.
[28] L. He, T.C. Ovaert, Heat partitioning coefficient calculations for sliding contacts with friction, Tribol. Trans. 51 (1) (2008) 12–18, https://doi.org/10.1080/10402000701739248.
[29] G. Zhang, et al., High thermal effusivity nanocarbon materials for resonant thermal energy harvesting, Small 17 (48) (2021), 2006752, https://doi.org/10.1002/smll.202006752.
[30] H. Mazidi, S. Jalalifar, J. Chakhoo, Mathematical modeling of heat conduction in a disk brake system during braking, Asian Journal of Applied Sciences 4 (2) (2011) 119–136, https://doi.org/10.3923/ajaps.2011.119.136.
[31] J. Wahlström, A pin-on-disc tribometer study of friction at low contact pressures and sliding speeds for a disc brake material combination, Results in Engineering 4 (2019), 100051, https://doi.org/10.1016/j.rineng.2019.100051.
[32] S. Oberst, J.C.S. Lai, in: Proceedings of 20th International Congress on Acoustics, Numerical Methods for Simulating Brake Squeal Noise, Sydney, Australia, 2010, pp. 23–27 (August).
[33] S. Oberst, J.C.S. Lai, S. Marburg, Guidelines for numerical vibration and acoustic analysis of disc brake squeal using simple models of brake systems, J. Sound Vib. 332 (9) (2013) 2284–2299, https://doi.org/10.1016/j.jsv.2012.11.034.
[34] H.L. Tsai, et al., in: Proceedings of the 14th National Computational Fluid Dynamics Conference, Transient thermal analysis of a disk brake system, New Taipei City, Taiwan, 2007, pp. 27–29.
[35] F. Cartigny, P. Dufrenoy, B. Desmet, A thermal analysis of a new railway brake concept using liquid cooling, Proc. Inst. Mech. Eng. - Part F J. Rail Rapid Transit 218 (2) (2004) 79–88, https://doi.org/10.1243/0954409041319605.
[36] T.P. Newcomb, Temperatures reached in disc brakes, J. Mech. Eng. Sci. 2 (3) (1960) 167–177, https://doi.org/10.1243/jmes_jour_1960_002_026_02.